Lateral nanoscale field emission comb for frequency mixing 🅕

L. B. De Rose ✉ 🄳 ; W. M. Jones 🄳 ; A. Scherer 🄳

Check for updates

CrossMark

View Online   Export Citation

Articles You May Be Interested In

On-chip dual-comb based on quantum cascade laser frequency combs

Appl. Phys. Lett. (December 2015)

Mapping of the Optical Frequency Comb to the Atom Velocity Comb

AIP Conference Proceedings (November 2006)

Frequency-modulated comb LIDAR

APL Photonics (October 2019)

AIP Publishing

Lateral nanoscale field emission comb for frequency mixing (F)

L. B. De Rose,[1,a)] (iD) W. M. Jones,[2,b)] (iD) and A. Scherer[1] (iD)

AFFILIATIONS

[1]Department of Applied Physics, California Institute of Technology, Pasadena, California 91125, USA
[2]Jet Propulsion Laboratory, California Institute of Technology, Pasadena, California 91109, USA

[a)]Author to whom correspondence should be addressed: lderose@caltech.edu
[b)]Present address: AWS Center for Quantum Computing, Pasadena, California 91125, USA.

ABSTRACT

Nanoscale field emission devices are promising candidates to design high-frequency electronics due to the lack of scattering in the vacuum channel that enables ballistic transport. In-plane devices are relatively easy to fabricate with current fabrication techniques and offer sub-fF capacitance. In this work, the characteristics of lateral gold multi-tip field emission arrays are studied. Vacuum gaps between the electrodes of 30 nm are fabricated, which allow < 10 V operation. The effect of number of emitting tips on measured current is investigated. By taking advantage of the strong non-linearity in the emission characteristic, frequency mixing in the MHz range is also demonstrated.

Field emission devices have been widely used for various applications, including as sources in electron microscopes and high-resolution electron beam lithography,[1,2] microwave power amplifiers,[3] flat panel displays,[4] x-ray sources,[5] pressure gauges,[6] and free-electron lasers.[7,8] Field emission-based technology is an attractive choice for designing electronic devices due to several reasons. First, vacuum devices are inherently resilient to extreme temperatures and radiation.[9,10] Continuous proper operation in harsh environments is crucial for applications in the automotive, nuclear, down-hole, and aerospace industries.[11,12] Moreover, unlike thermionic emission, field emission does not require heating, thus reducing power consumption and eliminating the need for thermal management. In addition, nanoscale vacuum gaps can be manufactured using either a top-down approach with current nanofabrication techniques and high-resolution electron lithography[13] or via a bottom-up approach using nanostructured materials such as nanocrystals, 2D materials, nanowires, and nanotubes.[14–18] This allows for operation at low voltages,[19] which is advantageous in terms of energy efficiency, Joule heating reduction, and minimizing the effects of ion sputtering that can result in device destruction.

Furthermore, field emission devices are promising candidates for high-frequency electronics due to their intrinsic superiority of vacuum as a transport medium that enables ballistic electron transport. In semiconductors, carriers suffer from acoustic and optical phonon scattering, which limits the maximum velocity a charge carrier can attain. The saturation velocity for Si is on the order of 1×10^7 cm/s, and for gallium arsenide, it is 1.2×10^7 cm/s, while the velocity of an electron in vacuum is theoretically about 3×10^{10} cm/s.[20] Thus, by fabricating the smallest nanoscale vacuum channels to shorten the electron transit time, field emission devices that operate at gigahertz frequencies or higher could be envisioned.[21] However, even though there have been multiple attempts to fabricate field emission devices for high-frequency operation, most of them have employed traditional Spindt-type vertical field emitter arrays, which have a large overlapping area between the gate and base electrodes. As a result of their high capacitance, their maximum frequency of operation has been limited to a few gigahertz.[22,23]

In this study, we propose to develop lateral symmetric field emission devices to minimize the overlapping area between the electrodes and, thus, reduce the capacitance compared to vertical geometries. Gold is selected as the electrode material due to its chemical unreactivity, ensuring that the value of the work function does not vary and affect emission stability, its high thermal and electrical conductivity, and the fact that liftoff is relatively easy and results in clean edges and reproducible fabrication. We will manufacture devices with many electron-emitting tips to source higher currents and to achieve stable emission, as the use of multiple tips should decrease flicker noise by ensemble averaging.[24] By taking advantage of the non-linear

current–voltage (IV) characteristic of field emission, which allows frequency conversion, we will design practical devices for heterodyning. In particular, we will fabricate a simple frequency mixer, an essential component in signal processing. Frequency mixers are widely employed in radar and high-bandwidth communication industries for military, radio astronomy, and civil use, as well as in high-speed transmitters and receivers in sensing systems.[25–27]

Field emission is the quantum-mechanical tunneling of electrons through the potential barrier at the surface of a material into vacuum by means of a high electric field.[28,29] This applied electric field causes the potential barrier at the interface to become narrow enough so that electrons have significant probability of tunneling into free-space. This emission mechanism is quantitatively described by the Fowler–Nordheim (FN) equation. In the simplest case for emission from a metallic surface, the current I is given by[30,31]

$$I = a_{FN} S \frac{E^2}{\phi} \exp\left(-\frac{b_{FN}\phi^{3/2}}{E}\right), \quad (1)$$

where S is the effective emission area, ϕ is the work function, E is the local electric field where emission takes place, and a_{FN} and b_{FN} are the so-called first and second FN field emission constants, respectively, given by

$$a_{FN} = \frac{e^3 m}{16\pi^2\hbar} \approx 1.54\ \mu A\,eV\,V^{-2},$$

$$b_{FN} = \frac{4}{3e}\sqrt{\frac{2m}{\hbar^2}} \approx 6.83\ V\,nm^{-1}eV^{-3/2},$$

where e and m are the elementary charge and mass of the electron, respectively. Moreover, the electric field can be expressed in terms of the applied voltage by $E = \gamma\frac{V}{d}$, where d is the separation between the emitter and collector terminals and γ is the field enhancement factor, a dimensionless parameter that depends on the emitter geometry. In practice, measured field emission IV data are often analyzed by means of the so-called FN plot, which allows us to quickly distinguish field emission characteristics from other emission mechanisms. In the FN plot, the y-axis is given by $\ln(I/V^2)$ and the x-axis by $1/V$, so that the field emission data in this semi-logarithmic plot form a straight line.

The devices were fabricated on a fused silica substrate due to its low loss tangent and cost. Direct-write electron beam lithography (Raith EBPG 5200) was used to pattern the devices at an acceleration voltage of 100 keV. The 50 Ω coplanar waveguides to couple the input signal into the devices were also designed. Note that a 25 nm chrome layer was previously evaporated to act as a charge dissipation layer during lithography and subsequently removed. Next, a 6 nm titanium adhesion layer, a 60 nm gold electrode layer, and a 20 nm titanium etch mask layer were deposited using electron beam evaporation at a pressure of $\sim 10^{-8}$ Torr (Kurt J. Lesker Labline), followed by overnight liftoff in acetone. Moreover, the insulating material in the vicinity of the emitting region was removed to avoid dielectric breakdown and device destruction, as well as to increase the length of the leakage pathway. This process was done in two steps: first, a dry etch with a C_4F_8 and O_2 chemistry was employed, followed by a short wet etch in buffered hydrofluoric acid to undercut the structures. To avoid damage from surface tension, the devices were gently dried using a critical point dryer (Tousimis 915B). Figure 1 shows an ion micrograph of the
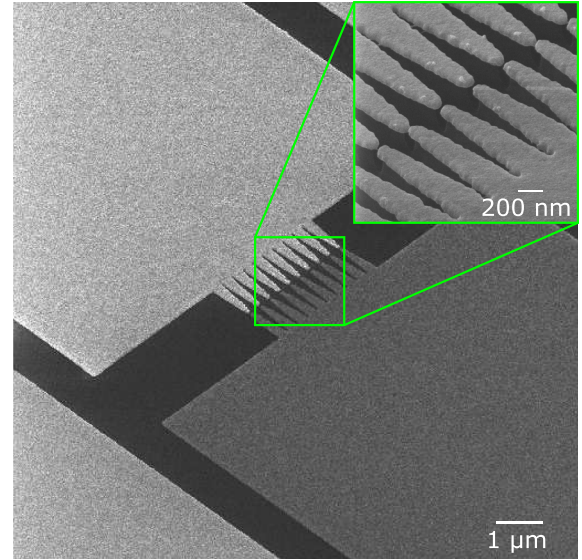

FIG. 1. Ion micrograph of the lateral field emission comb for a representative ten-tip device at 50° tilt. The separation between both electrodes is about 30 nm. The inset shows a magnified view of the device.

final structure. The distance between both electrical terminals is about 30 nm.

In order to prevent contamination that could affect emission stability, the devices were loaded into a stainless-steel vacuum chamber, which was pumped to a pressure of $\sim 10^{-6}$ Torr. The DC voltage needed to bias the field emission tips was provided by two picoammeter/voltage sources (Keithley 6487), which also monitored the emission current independently at each terminal to check that all currents were accounted for and there were no significant leakages. In addition, a pair of function generators supplied the AC voltage inputs (Keysight N5171B and Rohde & Schwarz SMC100A), which were coupled using a power combiner. A bias tee at the input of the device was used to superimpose both DC and AC signals, while another identical bias tee at the output was employed to deconvolute the two signals. Finally, the output time-varying signal was measured using a digital phosphor oscilloscope (Tektronix DPO7254). A schematic of the equivalent circuit for the measurement system is depicted in Fig. 2.
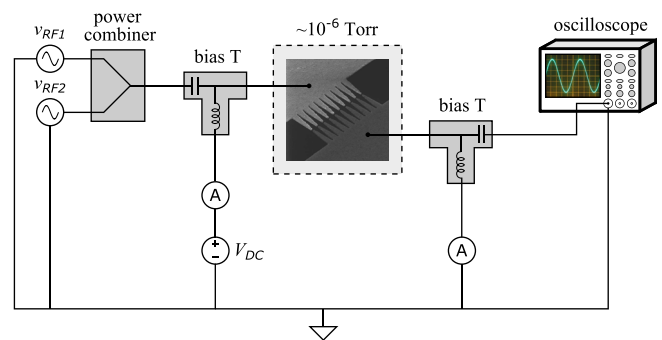

FIG. 2. Schematic of the test circuitry for frequency mixing.

The effect of the number of field emission tips on the measured current was examined. For this measurement, the DC power supplies were connected, and the AC lines were shorted. Multiple IV scans per device were taken until there was no significant change between consecutive runs to remove possible adsorbates from the emission surface. Figure 3(a) displays the IV characteristics of the fabricated field emission combs as a function of the number of tips per device. Note that a maximum current of 10 nA per tip was deliberately imposed to prevent overheating and potential damage. The devices displayed turn-on voltages under 10 V. Moreover, it was shown that, at a given applied bias, the measured current increased as a function of the number of emitter tips. Therefore, by increasing the number of tips per emitter, the turn-on voltage for electron emission was lowered, which is beneficial in terms of power consumption and lifetime considerations. In addition, sourcing higher DC currents at a given bias is desirable to enhance the performance of frequency conversion devices and achieve a higher conversion gain.
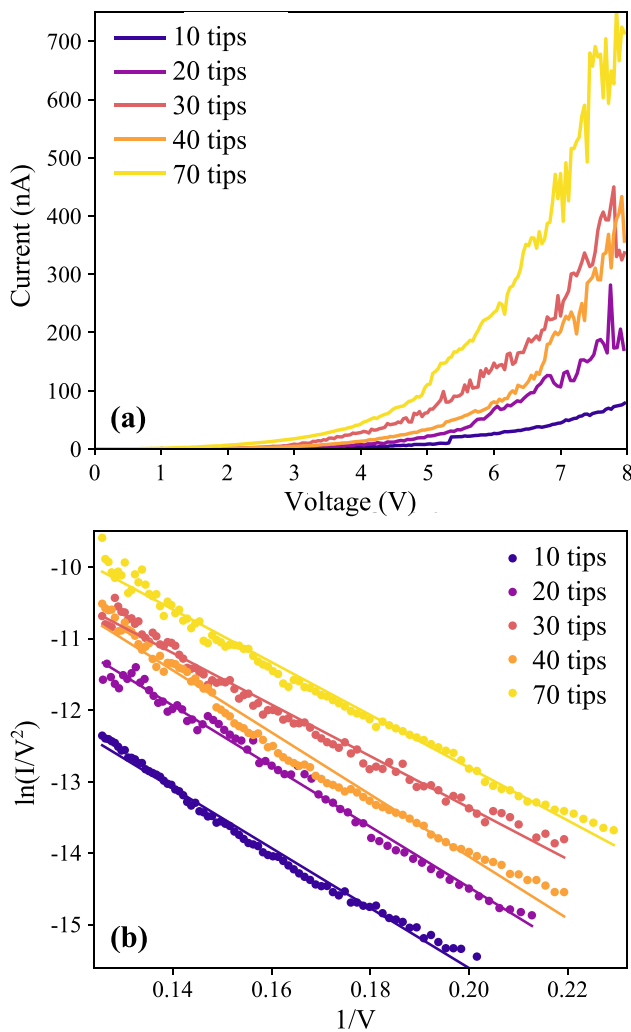
Furthermore, the data were plotted using FN coordinates, as illustrated in Fig. 3(b). Currents lower than 10% of the maximum measured current were ignored, as these are usually associated with other types of emission such as FP leakage,[32] unaccounted resistance paths,[33] or Schottky emission.[34] A linear model was well fit to the measured data, affirming the FN emission process. As the multi-tip array is equivalent to having many individual emitters in parallel, the overall FN current for the multi-tip array, I_{MT}, can be expressed in terms of a single-tip emitter current, I_{ST}, as

$$I_{MT} = nAV^2 \exp\left(-B/V\right), \qquad (2)$$
$$\equiv nI_{ST}, \qquad (3)$$

where n is the number of emitter tips and A and B are parameters that depend on, among others, the emission area, field enhancement factor, and work function. In FN coordinates, this becomes

$$\ln\left(\frac{I_{MT}}{V^2}\right) = \ln\left(nA\right) - B\left(\frac{1}{V}\right). \qquad (4)$$

Roughly the same slope was obtained from the linearization of the measured data for all devices. This agrees with Eq. (4), as the slope is independent of the number of emitter tips. From the slope, we can also calculate the field enhancement factor γ as 63 ± 5, which indicates that it does not vary significantly between devices. Furthermore, the magnitude of the y-intercept decreased as the number of emitter tips per device increased, also in agreement with Eq. (4), as the vertical intercept of a multi-tip device changes by a fixed amount given by $\ln(n)$ compared to single-tip emission. Using the y-intercept value of the ten-tip device, the efficient number of emitter tips was calculated and presented in Table I, alongside the values for the slope, y-intercept, field enhancement factor γ, turn-on electric field, and R^2 of the least squares regression line. Note that the turn-on field was defined as the required field to measure a current of 10 nA for ease of comparison between devices. A smaller value of effective emitter tips was expected due to fabrication discrepancies between gaps and roughness of individual tips, which cause only a fraction of the fabricated tips per device to turn on at a given bias and dominate emission. However, a higher effective number of tips than the actual number of tips was observed for some devices. Note that the analysis in Eq. (2) assumed an equal field enhancement factor and emission area for all tips. Although this may appear to be an oversimplification, due to the highly sensitive dependence of field emission on the atomic structure of the emitter tip, it is difficult, if not impossible, to attain controllable emission between different devices.[35] Thus, the devices with a larger effective

FIG. 3. Electrical characterization as a function of the number of tips per device: (a) IV characteristic and (b) FN plot.

TABLE I. Linear regression analysis data as a function of the number of tips.

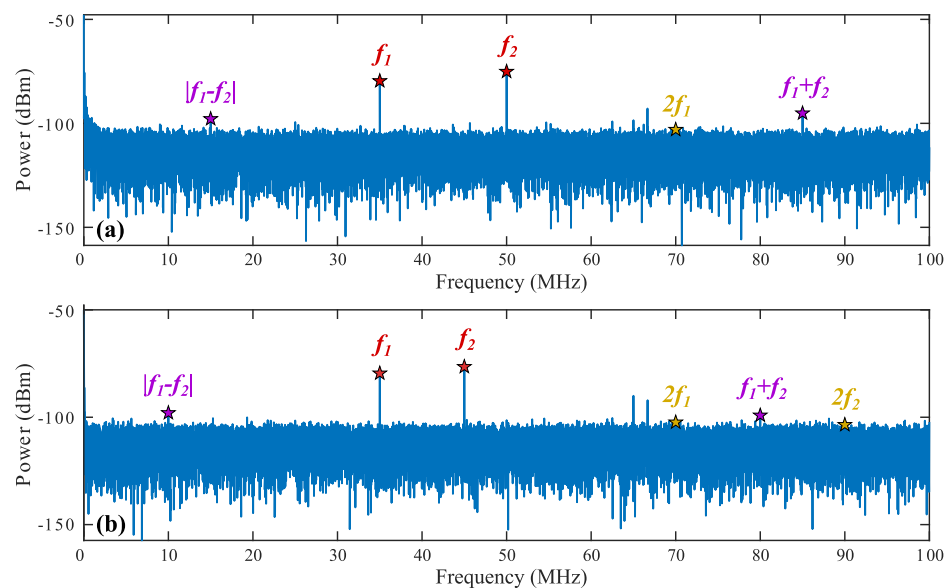| Number of tips	Slope	y-intercept	Number of tips (effective)	Field enhancement factor γ	Turn-on field (V/nm)	R^2 value
10	−41.82	−7.235	10	60	10.6	0.989
20	−42.24	−6.023	33	59	8.49	0.990
30	−35.97	−6.166	29	70	7.48	0.985
40	−43.30	−5.383	63	58	7.11	0.981
70	−37.27	−5.370	64	67	5.41	0.988

FIG. 4. Power spectra of the output signal for mixing experiment. The DC voltage was ∼5.5 V, and the measured current was 350 nA. The amplitude of each AC signal was 1 V$_{RMS}$. (a) $f_1 = 35$ MHz and $f_2 = 50$ MHz; (b) $f_1 = 35$ MHz and $f_2 = 45$ MHz.

number of tips may had a smaller effective emission area as a result of nanoprotrusions created during fabrication.

Next, we calculated an estimate for the cutoff frequency of the specific device under test that would be employed during the frequency mixing experiment, which we selected to be the ten-tip device. A static analysis was used to determine the dynamic impedance of the device by differentiating the IV characteristic right before the AC tests were carried out. A value of 0.67 MΩ was obtained at the fixed current level that would be later sourced, namely, 350 nA. A simulation using COMSOL Multiphysics yielded a value of 240 aF for the device capacitance. Thus, we estimate an RC cutoff frequency[36] of ∼1 GHz. In order to obtain a higher cutoff frequency, the dynamic impedance of the device can be reduced by sourcing higher currents at a given bias. This can be achieved by increasing the number of tips per emitter, coating the device with a low work function material, or reducing the vacuum gap between the electrodes, among others.

Finally, based on the estimate for the cutoff frequency of the specific device under test, we proceeded with the frequency mixing experiment. Two AC signals with an amplitude of 1 V$_{RMS}$ at frequencies $f_1 = 35$ MHz and $f_2 = 50$ MHz were superimposed on the DC bias of ∼5.5 V. Figure 4(a) shows the power spectrum obtained by computing the fast Fourier transform with the oscilloscope. Power values at all

frequencies of interest are included in Table II. We observed peaks at the sum ($f_1 + f_2 = 85$ MHz) and difference ($|f_1 − f_2| = 15$ MHz) frequencies, confirming that the field emitter array achieved frequency mixing. The conversion loss was about 108 dBm as a result of the high impedance of the device. However, this value only serves as a worst-case scenario as the input signal frequencies were not matched to the device. Thus, significantly better results are expected if impedance matching is attempted. We also changed the input frequencies to $f_1 = 35$ MHz and $f_2 = 45$ MHz and measured similar results as illustrated in Fig. 4(b). Finally, we confirmed that no peaks at the sum or difference were present when the device was "off" (i.e., no DC bias was applied and no field emission current was measured), but the AC sources were turned on, as well as that no peaks at the input frequencies f_1

TABLE II. Measured power for all frequencies of interest shown in Fig. 4.

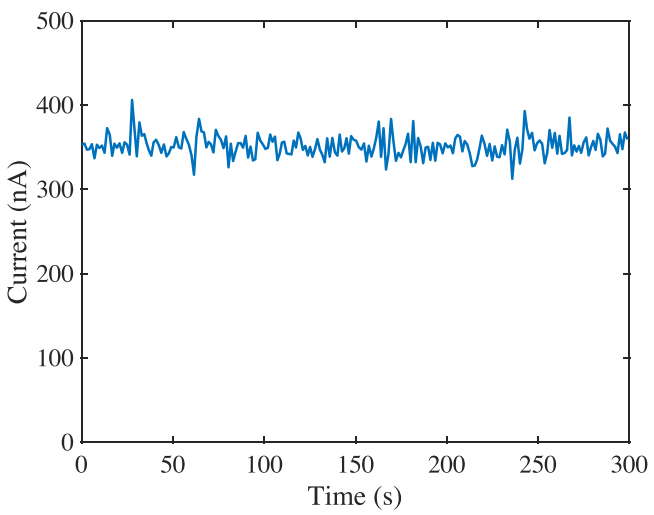| Plot label | Fig. 4(a) | | Fig. 4(b) | |
	Frequency (MHz)	Power (dBm)	Frequency (MHz)	Power (dBm)
f_1	35	−79.6	35	−79.5
f_2	50	−75.1	45	−76.5
$f_1 + f_2$	85	−95.1	80	−99.1
$|f_1 − f_2|$	15	−97.9	10	−98.0

FIG. 5. Stability of the measured DC field emission current during mixing experiment.

and f_2 were measured when the device was "on" (i.e., DC bias was applied and field emission current was measured), but the AC sources were switched off. Additionally, the stability of the measured DC during the duration of the mixing experiment is shown in Fig. 5. Unfortunately, the device exploded before mixing at higher frequencies was attempted.

In this work, we discussed the fabrication and experimental characterization of lateral multi-tip field emission arrays with nanoscale vacuum separation between electrodes. Even though the devices were manufactured using gold, the fabrication process can also be extended to other metals that can be evaporated. We have demonstrated < 10 V operation as well as a significant increase in the emission current as a function of the number of emitting tips. Frequency mixing in the MHz range was also reported with an expected cutoff frequency of $\sim$1 GHz. The impedance of the proposed structure could be reduced by fabricating more tips per device to source higher currents at a given bias, allowing for higher maximum operating frequency.

AUTHOR DECLARATIONS
Conflict of Interest

The authors have no conflicts to disclose.

Author Contributions

Lucia Belen De Rose: Conceptualization (equal); Formal analysis (lead); Investigation (lead); Methodology (lead); Software (equal); Writing – original draft (lead); Writing – review & editing (lead). **William Maxwell Jones:** Conceptualization (equal); Funding acquisition (lead); Investigation (supporting); Methodology (supporting); Software (equal); Writing – review & editing (supporting). **Axel Scherer:** Funding acquisition (supporting); Supervision (lead); Writing – review & editing (supporting).

DATA AVAILABILITY

The data that support the findings of this study are available from the corresponding author upon reasonable request.

REFERENCES

[1]G. N. Fursey, "Field emission in vacuum micro-electronics," Appl. Surf. Sci. **215**, 113–134 (2003).

[2]G. Gaertner, W. Knapp, and R. G. Forbes, *Modern Developments in Vacuum Electron Sources* (Springer Cham, 2020).

[3]D. R. Whaley, B. Gannon, C. R. Smith, C. M. Armstrong, and C. A. Spindt, "Application of field emitter arrays to microwave power amplifiers," IEEE Trans. Plasma Sci. **28**, 727–747 (2000).

[4]A. A. Talin, K. A. Dean, and J. E. Jaskie, "Field emission displays: A critical review," Solid State Electron. **45**, 963–976 (2001).

[5]P. R. Schwoebel, "Field emission arrays for medical x-ray imaging," Appl. Phys. Lett. **88**, 113902 (2006).

[6]R. Baptist, C. Bieth, and C. Py, "Bayard–Alpert vacuum gauge with microtips," J. Vac. Sci. Technol. B **14**, 2119–2125 (1996).

[7]X. Li, M. Li, L. Dan, Y. Liu, and C. Tang, "Cold cathode RF guns based study on field emission," Phys. Rev. Accel. Beams **16**, 123401 (2013).

[8]F. Floreani, H. W. Koops, and W. Elsäßer, "Concept of a miniaturised free-electron laser with field emission source," Nucl. Instrum. Meth. A **483**, 488–492 (2002).

[9]L. Wang, G. Wei, F. Gao, C. Li, and W. Yang, "High-temperature stable field emission of B-doped SiC nanoneedle arrays," Nanoscale **7**, 7585–7592 (2015).

[10]L. B. De Rose, A. Scherer, and W. M. Jones, "Suspended nanoscale field emitter devices for high-temperature operation," IEEE Trans. Electron Devices **67**, 5125–5131 (2020).

[11]P. L. Dreike, D. M. Fleetwood, D. B. King, D. C. Sprauer, and T. E. Zipperian, "An overview of high-temperature electronic device technologies and potential applications," IEEE Trans. Compon. Pack. A **17**, 594–609 (1994).

[12]J. Watson and G. Castro, "A review of high-temperature electronics technology and applications," J. Mater. Sci. Mater. Electron. **26**, 9226–9235 (2015).

[13]S. M. Lewis, M. S. Hunt, G. A. D. H. R. Alty, J. Li, A. Wertheim, L. De Rose, G. A. Timco, A. Scherer, S. G. Yeates, and R. E. P. Winpenny, "Plasma-etched pattern transfer of sub-10 nm structures using a metal–organic resist and helium ion beam lithography," Nano Lett. **19**, 6043–6048 (2019).

[14]L. Iemmo, A. Di Bartolomeo, F. Giubileo, G. Luongo, M. Passacantando, G. Niu, F. Hatami, O. Skibitzki, and T. Schroeder, "Graphene enhanced field emission from InP nanocrystals," Nanotechnology **28**, 495705 (2017).

[15]A. Grillo, M. Passacantando, A. Zak, A. Pelella, and A. Di Bartolomeo, "WS$_2$ nanotubes: Electrical conduction and field emission under electron irradiation and mechanical stress," Small **16**, 2002880 (2020).

[16]C. C. Chiu, T. Y. Tsai, and N. H. Tai, "Field emission properties of carbon nanotube arrays through the pattern transfer process," Nanotechnology **17**, 2840 (2006).

[17]X. Li and J. Feng, "Review of nanoscale vacuum devices," Electronics **12**, 802 (2023).

[18]J. Li, W. Lei, X. Zhang, B. Wang, and L. Ba, "Field emission of vertically-aligned carbon nanotube arrays grown on porous silicon substrate," Solid State Electron. **48**, 2147–2151 (2004).

[19]W. M. Jones, D. Lukin, and A. Scherer, "Practical nanoscale field emission devices for integrated circuits," Appl. Phys. Lett. **110**, 263101 (2017).

[20]J. W. Han, J. S. Oh, and M. Meyyappan, "Cofabrication of vacuum field emission transistor (VFET) and MOSFET," IEEE Trans. Nanotechnol. **13**, 464–468 (2014).

[21]H. G. Kosmahl, "A wide-bandwidth high-gain small-size distributed amplifier with field-emission triodes (FETRODEs) for the 10 to 300 GHz frequency range," IEEE Trans. Electron Dev. **36**, 2728–2737 (1989).

[22]C. A. Spindt, C. E. Holland, A. Rosengreen, and I. Brodie, "Field-emitter-array development for high-frequency operation," J. Vac. Sci. Technol. B **11**, 468–473 (1993).

[23]J. H. Nam, H. S. Uh, J. D. Lee, J. D. Ihm, Y. H. Kim, and K. M. Choi, "Characteristics and circuit model of a field emission triode," J. Vac. Sci. Technol. B **16**, 916–919 (1998).

[24]S. Yamamoto, "Fundamental physics of vacuum electron sources," Rep. Prog. Phys. **69**, 181 (2005).

[25]I. Mehdi, J. V. Siles, C. Lee, and E. Schlecht, "THz diode technology: Status, prospects and applications," Proc. IEEE **105**, 990–1007 (2017).

[26]B. Henderson and E. Camargo, *Microwave Mixer Technology and Applications* (Artech House, 2013).

[27]P. Horowitz and W. Hill, *The Art of Electronics* (Cambridge University Press, 1986).

[28]A. Modinos, *Field, Thermionic and Secondary Electron Emission Spectroscopy* (Springer, 1984).

[29]R. Gomer, *Field Emissions and Field Ionization* (American Institute of Physics, 1993).

[30]G. Fursey, *Field Emission in Vacuum Microelectronics* (Springer, 2005).

[31]S. D. Liang, *Quantum Tunneling and Field Electron Emission Theories* (World Scientific, 2014).

[32]A. Di Bartolomeo, F. Giubileo, L. Iemmo, F. Romeo, S. Russo, S. Unal, M. Passacantando, V. Grossi, and A. M. Cucolo, "Leakage and field emission in side-gate graphene field effect transistors," Appl. Phys. Lett. **109**, 023510 (2016).

[33]R. G. Forbes, "Development of a simple quantitative test for lack of field emission orthodoxy," Proc. R. Soc. A **469**, 20130271 (2013).

[34]M. Turchetti, Y. Yang, M. Bionta, A. Nardi, L. Daniel, K. K. Berggren, and P. D. Keathley, "Electron emission regimes of planar nano vacuum emitters," IEEE Trans. Electron Dev. **69**, 3953–3959 (2022).

[35]G. Wu, X. Wei, S. Gao, Q. Chen, and L. Peng, "Tunable graphene microemitters with fast temporal response and controllable electron emission," Nat. Commun. **7**, 11513 (2016).

[36]R. E. Neidert, P. M. Phillips, S. T. Smith, and C. A. Spindt, "Field emission triodes," IEEE Trans. Electron Dev. **38**, 661–665 (1991).

27 October 2023 21:58:06